Sensors and Materials, Vol. 38, No. 3 (2026) 1181–1191
MYU Tokyo

S & M 4370

Liquid Layer Thickness Maintenance and Regulation in Gas-phase Odor Biosensor

Hongchao Deng,[1] Chao Yang,[1] Jianbing Zheng,[1]
Heng Su,[2] Zhangyu Chen,[3*] and Takamichi Nakamoto[4]

[1]Zhejiang Huanmao Auto-Control Technology Co., Ltd.,
Lianchuang Avenue No. 199, Wuchang, Yuhang, Hangzhou 311121, China
[2]Suichang Environmental Protection Monitoring Station, Gongyuan Road No. 89, Suichang, Lishui 323300, China
[3]Zhejiang Ecological Environment Group,
Lianchuang Avenue No. 199, Wuchang, Yuhang, Hangzhou 311121, China
[4]Institute of Integrated Research, Institute of Science Tokyo,
4259 Nagatsuta-cho, Midori, Yokohama, Kanagawa 226-8503, Japan

(Received December 25, 2025; accepted January 28, 2026)

Keywords: liquid layer, gas phase, odor biosensor, open-loop control, closed-loop control, olfactory receptor

Most biological materials utilized in odor biosensors require an aqueous environment for retaining their function. However, the buffer medium surrounding the sensing materials can be a barrier for hydrophobic odorant molecules to penetrate. There are two methods to solve this problem. The first is the addition of molecular transporters, e.g., odorant binding proteins. The second is to cover the sensing materials with a sufficiently thin liquid layer. Considering that a thin liquid layer is easy to realize and inexpensive, we focused on this approach for direct gas-phase odor sensing. Here, we present diverse methods—no additional control, open-loop control, and closed-loop control—for maintaining a thin liquid layer in the odor biosensor. We recorded the impedance curve under liquid natural evaporation and proposed an impedance equivalent circuit model. We investigated the reason for the early stopping of the biosensor response. Moreover, we demonstrated the performance of a suitable closed-loop control method in fine tuning the liquid layer thickness. The methods reported in this paper would contribute to enabling the practical application of odor biosensors.

1. Introduction

Multiple types of sensing materials have been utilized in odor biosensors, e.g., olfactory receptor (OR) protein,[(1)] odorant binding protein (OBP),[(2)] cell expressing OR,[(3–5)] and olfactory sensory neuron (OSN).[(6)] All these materials require an aqueous environment to maintain their function.[(7–9)] Therefore, these biosensors were submerged in buffer medium, and their target odorants were dissolved in an organic solvent, then applied. In the gas-phase odorant detection, hydrophobic odorant molecules cannot penetrate through the thick buffer solution layer. To solve

*Corresponding author: e-mail: chenzy@zjepb.gov.cn
https://doi.org/10.18494/SAM6133

ISSN 0914-4935
https://myukk.org/

this problem, additional molecular transporters or an adequately thin liquid layer is necessary.[10,11]

The mucus layer in the human airway has a thickness ranging from 0.5 to 5 μm and diverse OBPs are secreted into it.[12] Odorant molecules can easily pass through this mucus layer and then bind with OR. Compared with producing and purifying the proper OBP,[13] maintaining a relatively thin liquid layer is easy and cheap. Without liquid layer thickness control, the buffer solution will quickly dry out, leading to a short biosensor lifetime.[4] A buffer layer containing agarose or collagen lasts longer while the buffer medium still evaporates.[14,15] To solve this problem, liquid layer thickness control is essential. Both the open-loop and closed-loop control methods are suitable for resolving this issue; the differences mainly lie in the precision of control and the complexity of the structure.

In this manuscript, we describe no control, open-loop control, and closed-loop control methods for the gas-phase odor biosensor liquid layer thickness. The liquid layer thickness was evaluated using the impedance of two electrodes immersed in the buffer medium. We analyzed the early stopping of biosensor response and exchanged the liquid to mitigate the effect of residual odorant on the biosensor response. Reproducible biosensor responses under direct gas-phase odorant stimulation were obtained. Finally, the fine tuning of the liquid layer thickness was achieved with variable impedance set points.

2. Materials and Methods

2.1 Experiment system

The experiment system is shown in Fig. 1. An air pump (RWP16B08RG, Oken Seiko) blew air to a solenoid valve (EXAK-3, Takasago Denki). A microcontroller (Arduino Nano, Arduino) determined whether air was discarded or flowed to the odorant sample bottle. The headspace gas of the odorant sample was used to stimulate the sensing material, i.e., a cell expressing OR.[5,16] The liquid layer thickness was under the no control, open-loop control, or closed-loop control condition. In open-loop control, a syringe pump (LPDA2750125D, Lee Company) was selected to supply the liquid at a fixed rate. In closed-loop control, one or two syringe pumps were adopted for adjustable-rate liquid compensation. Two electrodes were in contact with the buffer medium and the impedance between them indicated the liquid layer thickness. The real-time impedance was input into another microcontroller (Arduino Nano, Arduino) for adjusting the pumping rate under closed-loop control. Cell images were recorded with a camera (OV7740, OmniVision) and processed by a system-on-chip (SoC) field-programmable gate array (FPGA) board (DE1-SoC 5CSEMA5, Altera). The overall cell brightness variation was utilized to calculate the biosensor response.

2.2 Sensing material

The sensing material was described in detail in our previous papers.[17,18] In brief, the Sf21 cell derived from *Spodoptera frugiperda* expressing OR, OR coreceptor (Orco), and GCaMP6s

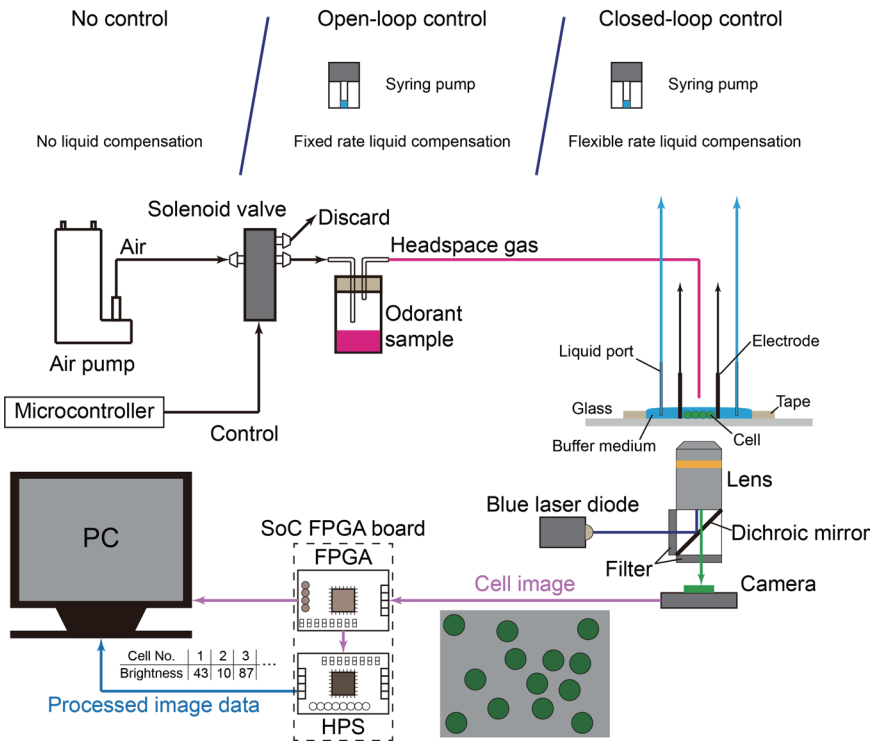

Fig. 1. (Color online) Structure of the experiment system. The liquid layer thickness was under the no control, open-loop control, or closed-loop control condition.

protein was chosen for our experiments.[19] The OR was Or13a from *Drosophila melanogaster.* The OR and Orco formed a ligand-gated ion channel. This channel is open, resulting in a calcium ion influx when the target ligand—1-octen-3-ol (O5284, Sigma-Aldrich)—is captured by Or13a.[20] GCaMP6s is a calcium-sensitive fluorescent protein and its fluorescence intensity increases with the calcium ion concentration.[19] The relative increase in cell brightness before and after odor stimulation was regarded to be a biosensor response. Since the focus of this paper is not the improvement of the biosensor performance, further description related to sensor features can be found in our former research reports.[21,22]

2.3 Experimental procedure

Before beginning an experiment, all peripherals were set, the target odorant was added to the sample bottle, and cells expressing OR were loaded into the experiment area. The odorant sample was pure 1-octen-3-ol diluted with mineral oil. If not specially stated, the odorant sample concentration was the volume ratio after dilution, usually 0.1 or 1%. Depending on the liquid layer thickness control method, there was no liquid compensation under the no control condition,[4] fixed flow rate liquid compensation under the open-loop control condition, or adjustable flow rate liquid compensation under the closed-loop control condition.[23] The compensated liquid was deionized water or Ringer's solution (140 mM NaCl, 5.6 mM KCl, 4.5 mM $CaCl_2$, 11.26 mM $MgCl_2$, 11.32 mM $MgSO_4$, 9.4 mM D-glucose, 5 mM HEPES, pH 7.2).

The cell images were captured and used for analyzing the cell state and biosensor responses.[17] Moreover, the impedance between two electrodes was recorded using a homemade measurement circuit.[24] The core component of this circuit was an impedance converter (AD5933, Analog Devices), with a calibration impedance (usually 1 kΩ). The impedance absolute value under 10 to 100 kHz measurement frequency can be obtained. After the experiment, the experiment area was completely rinsed with deionized water for the next test.

3. Results and Discussion

3.1 No control condition

Under the no control condition, the buffer solution containing cells naturally evaporated and the impedance increased continuously. Our impedance measurement circuit can measure the impedance from 10 to 100 kHz at 1 kHz intervals. A typical impedance curve is presented in Fig. 2(a). Although only few measurement results are displayed, the impedance tendencies are similar among all measurement frequencies. Considering that a higher measuring frequency equals a shorter sampling duration, we selected 100 kHz.

Figure 2(b) shows detailed information about the experiment area. A piece of tape with a 5 × 5 mm^2 hole was pasted on a glass slide. Six microliters of Ringer's solution with cells was loaded into the experiment area; hence, the estimated liquid layer thickness was 240 μm. The tip of the electrodes in contact with the buffer medium was a cone (height around 600 μm). Figure 2(c)

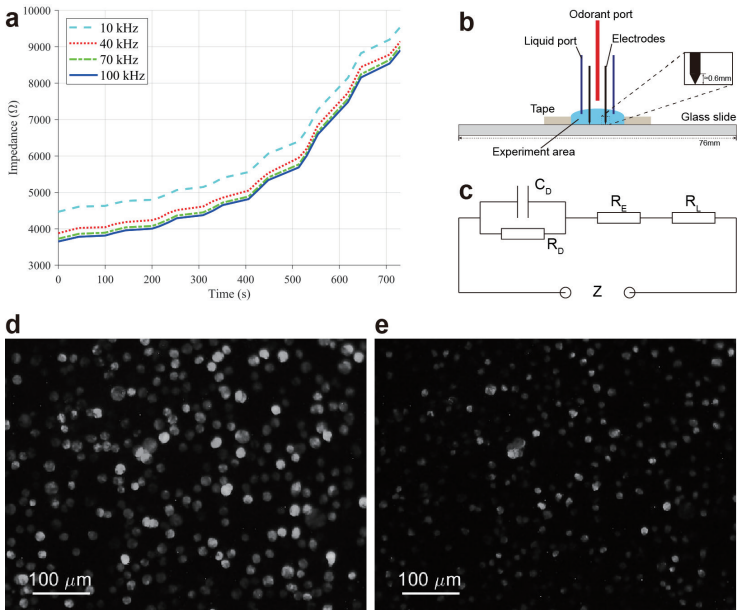

Fig. 2. (Color online) Biosensor performance under no control condition. (a) Typical impedance variation during experiment. The presented measurement frequencies were 10, 40, 70 and 100 kHz. (b) Detailed information about the experiment area. (c) Equivalent circuit model of impedance measurement. (d) Cell image at the beginning of the experiment. (e) Cell image 1300 s after the start of the experiment.

shows the equivalent circuit model of the impedance measured in the experiments. In this circuit, the overall impedance Z is described as

$$Z = C_D // R_D + R_E + R_L, \tag{1}$$

where C_D, R_D, R_E, R_L, and Z denote the impedance measurement circuit internal capacitance, impedance measurement circuit internal resistance, electrode resistance, assay buffer solution resistance, and overall impedance, respectively. C_D, R_D, and R_E are constants in individual experiments, whereas R_L depends on the medium solution in the cell area. R_L is expressed as

$$R_L = \frac{L}{A}\rho, \tag{2}$$

where L is the distance between the electrodes, A the contact area between an electrode and a liquid layer, and ρ the resistivity. Because the tip of the electrode is a cone, the contact area can be calculated as

$$A = \pi \cdot r \cdot l, \tag{3}$$

where r is the bottom radius and l the slant height. At time T_0, the liquid layer thickness is h_0, and the radius and slant height of the partial cone submerged in the liquid are r_0 and l_0, respectively. h_0 is proportional to r_0 and l_0; thus,

$$r_0 \cdot l_0 = k \cdot h_0^2. \tag{4}$$

Since the NaCl concentration is much higher than the concentrations of the other components in the assay buffer solution, we can assume that this medium is essentially a solution containing one electrolyte. Therefore, the resistivity is determined as

$$\rho = \frac{1}{\Lambda_m \cdot c}, \tag{5}$$

where Λ_m is the molar conductivity and c the electrolyte concentration. The electrolyte concentration at time T_0 is c_0.

Integrating from Eqs. (2) to (5), the assay buffer solution resistance at time T_0 equals

$$R_{L,T_0} = \frac{L}{\pi k h_0^2} \cdot \frac{1}{\Lambda_m \cdot c_0}. \tag{6}$$

At time T_1, as the liquid layer thickness decreased Δh owing to water evaporation, the new buffer solution resistance becomes

$$R_{L,T_1} = \frac{L}{\pi k (h_0 - \Delta h)^2} \cdot \frac{1}{\Lambda_m \cdot c_0 \frac{h_0}{h_0 - \Delta h}}. \tag{7}$$

Therefore, the increase in resistance is

$$\Delta R_L = \frac{L}{\pi k h_0^2 \Lambda_m c_0} \cdot \frac{\Delta h}{h_0 - \Delta h}. \tag{8}$$

According to Eq. (8), when $h_0 \gg \Delta h$, the impedance change is proportional to the change in liquid layer thickness. That is, the impedance changes linearly with time. When the liquid layer becomes much thinner, a small thickness variation leads to a large impedance change. This is in line with the impedance curve in Fig. 2(a): the impedance rose slowly with time before 400 s, after which the gradient became much larger.

Under the no control condition, the experiment preparation was simple while always encountering liquid dry-out problems. Without sufficient buffer solution, the cell brightness and shape varied considerably and showed no response to odor stimulation [Figs. 2(d) and 2(e)]. Such a short biosensor lifetime limits its application in long-term continuous monitoring.(4)

3.2 Open-loop control condition

An easy way to maintain the liquid film is open-loop control, namely, adding liquid into the experiment area at a fixed flow rate. Under this condition, a syringe pump was utilized for supplying the buffer solution into the experiment area. Figure 3(a) shows a favorable result of reproducible biosensor responses under open-loop control. With liquid compensation, the cells maintained their normal morphology for a longer period [Figs. 3(d) and 3(e)], and the biosensor lifespan was extended to around 30 min.

However, the liquid evaporation speed is affected by diverse environmental factors, e.g., temperature, humidity, and gas flow speed. It is difficult to determine a suitable compensation speed. Also, successful results similar to that shown in Fig. 3(a) are the minority among all experiment outcomes. Two examples of test outcomes are shown in Figs. 3(b) and 3(c). In Fig. 3(b), the liquid compensation speed was very low, so the liquid in the experiment area dried out and a large abnormal peak appeared in the later part of the fluorescent intensity curve. In Fig. 3(c), too much buffer medium was supplied, so the response diminished until it became invisible. These results demonstrate that extending the cell lifetime through open-loop control was insufficient to obtain our desired outputs. A better method is earnestly required.

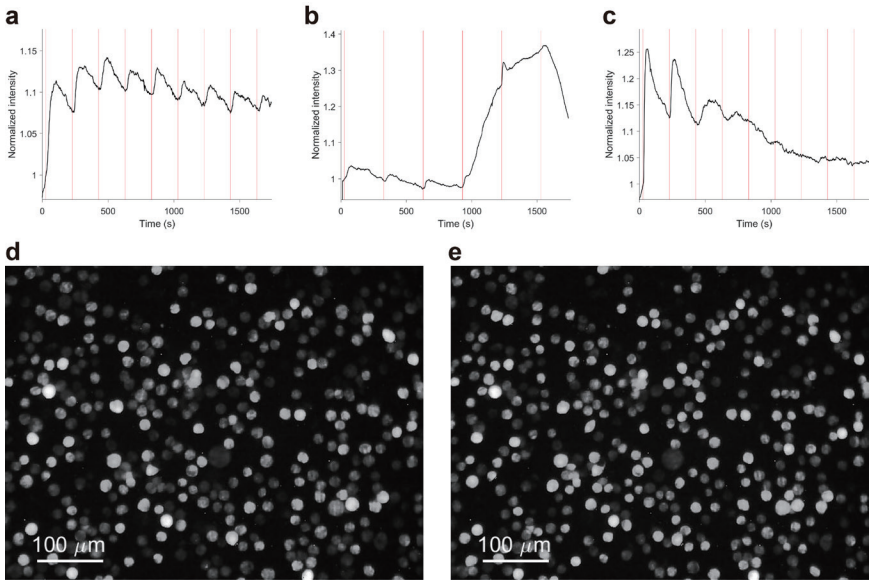

Fig. 3. (Color online) Biosensor performance under open-loop control condition. (a) Good result of biosensor response to 0.4 s 0.1% 1-octen-3-ol headspace vapor stimulation. The red vertical lines indicate the timing of vapor exposure. (b) The liquid compensation speed was very low. The odorant was 0.4 s 0.1% 1-octen-3-ol headspace vapor. The red vertical lines indicate the timing of vapor exposure. (c) The liquid compensation speed was very high. The odorant was 0.4 s 0.1% 1-octen-3-ol headspace vapor. The red vertical lines indicate the timing of vapor exposure. (d) Cell image at the beginning of the experiment. (e) Cell image 1764 s after the start of the experiment.

3.3 Closed-loop control condition

Closed-loop control, which is also called feedback control, was more suitable for the task here. It adjusted the liquid supplementation rate in accordance with the real-time measurement result. A schematic diagram of closed-loop control is shown in Fig. 4(a). The liquid layer thickness was evaluated from the impedance between the electrodes. The set point of this feedback control structure can be the impedance at the beginning of the experiment or adjustable during the test. The error between the set point and the real-time impedance was collected by the microcontroller. In the microcontroller, the proportional-integral-derivative (PID) algorithm generated a control signal to tweak the syringe pump. The syringe pump infused or withdrew the buffer medium, thus adjusting the liquid layer thickness. The current impedance was measured by the impedance measurement circuit.

Closed-loop control maintained a stable impedance, i.e., the liquid layer thickness, throughout the experiment. Nevertheless, the early stopping of the biosensor response still occurred under this condition [Fig. 4(b)]. There are two hypotheses regarding the reason for this outcome. The first was that pure water evaporated while ions remained in the experiment area, and the increased ion concentration inhibited the biosensor response. The second was that the residual odorant molecules from the former odor stimulations suppressed the subsequent biosensor responses. To test the first hypothesis, we replaced the compensation liquid from Ringer's solution to deionized water. Even though no additional ions were introduced during the

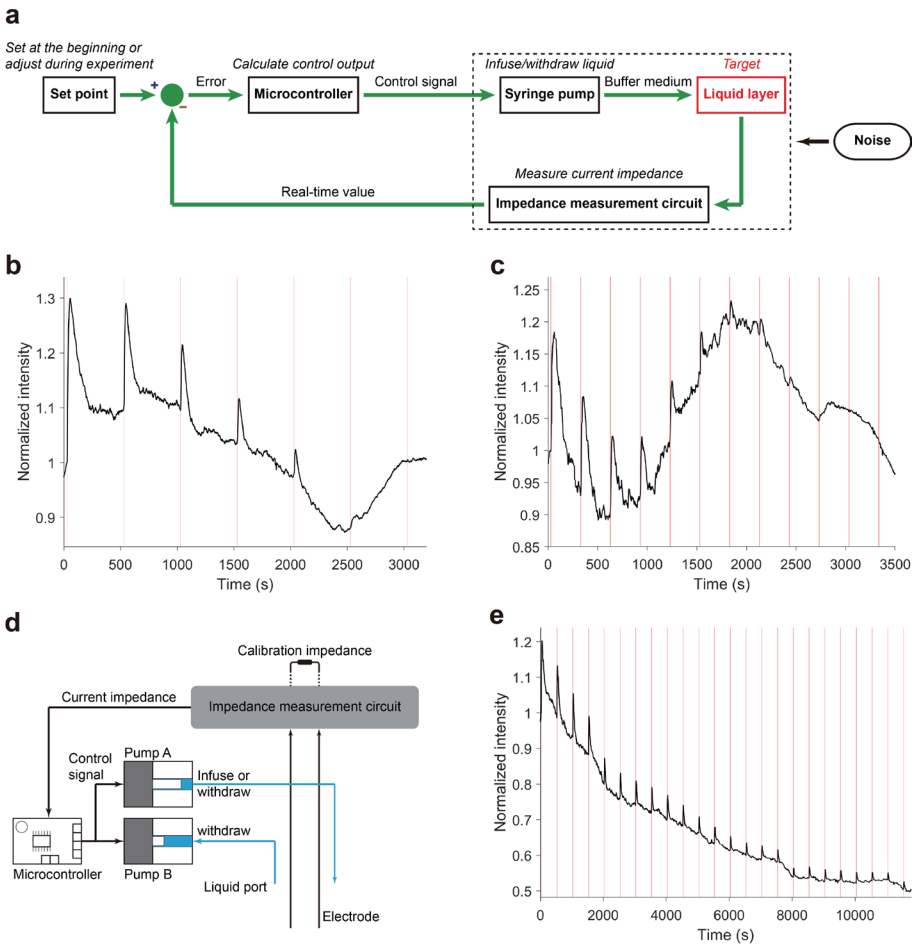

Fig. 4. (Color online) Biosensor performance under closed-loop control condition. (a) Schematic of closed-loop control. The noise mainly comes from the deviation of the impedance measurement. (b) Maintaining only the liquid layer thickness was insufficient to extend the biosensor lifespan. The odor stimulation was 0.4 s 1% 1-octen-3-ol headspace vapor. The red vertical lines indicate the timing of stimulations. (c) Using deionized water to compensate for the evaporated liquid. The biosensor lifetime was not markedly extended. The odor stimulation was 0.4 s 1% 1-octen-3-ol headspace vapor. The red vertical lines indicate the timing of stimulations. (d) Liquid exchange structure was realized by using two syringe pumps. (e) Liquid layer thickness control and liquid exchange can clearly extend the biosensor lifespan. The odor stimulation was 0.4 s 1% 1-octen-3-ol headspace vapor. The red vertical lines indicate the timing of stimulations. The withdrawing flow rate of pump B was 1.1116 μl/min.

experiment, the cell response terminated at the 6th stimulation, at around 2500 s [Fig. 4(c)]. This proved that the ion density increase was not the principal cause of the early stopping of the OR response. Moreover, the low osmotic pressure of deionized water caused cell swelling as well as the introduction of artifacts in the fluorescent intensity curve (result not shown here). For the second hypothesis, we exchanged the liquid in the experiment area by introducing another pump. As depicted in Fig. 4(d), the microcontroller controlled pumps A and B simultaneously. This approach can concurrently solve the residual ion and odorant hitches. Pump B only withdrew the liquid from the experiment area and pump A infused or withdrew liquid to keep the liquid film thickness constant. For the convenience of calculation, there was a default

pumping speed of pump A that was equal to the withdrawing speed of pump B. Hence, the withdrawing rate of pump B determined the liquid exchange rate. With liquid layer thickness control and liquid exchange, the biosensor lifetime was significantly extended [Fig. 4(e)]. The decrement trends of normalized intensity were mainly caused by the photobleaching of fluorescent protein. Under continuous odorant stimulations, the fluorescent protein responses typically decreased with time. This phenomenon was also observed in our previous study.[17]

3.4 Variable impedance during experiment

In Sect. 3.3, the set point of the feedback control structure was the impedance measured at the beginning of the experiment, whereby the liquid layer thickness was stable. By varying the impedance set points, the liquid layer thickness can be varied. Figure 5(a) shows an example of adjusted impedance during the experiment. The initial impedance set point was 2200 Ω and the impedance increased 25% every 500 s. When the impedance was stable, the PID output was positive and constant; thus, Ringer's solution was infused into the experiment area. Once the impedance set point was elevated, the PID output declined sharply and became a large negative value. Some of the buffer medium was extracted from the experiment area, whereby the real-time impedance increased towards the new set point. The alteration of the impedance set point resulted in a significant artifact in the fluorescent intensity curve. Hence, the timing of changing the impedance set point should be sufficiently separated from the timing of odor stimulation.

A higher impedance means a thinner liquid layer, which leads to a more robust biosensor response.[25] Unfortunately, Fig. 5(b) shows that when the impedance set point exceeds a threshold, the PID output turns into an abnormal negative value after 3700 s. With such a high impedance, the liquid layer was so thin that the liquid port connected to pump B could not withdraw any buffer medium. The default liquid pumping rate in pump A was very high for liquid evaporation compensation. To maintain the liquid film thickness, the microcontroller

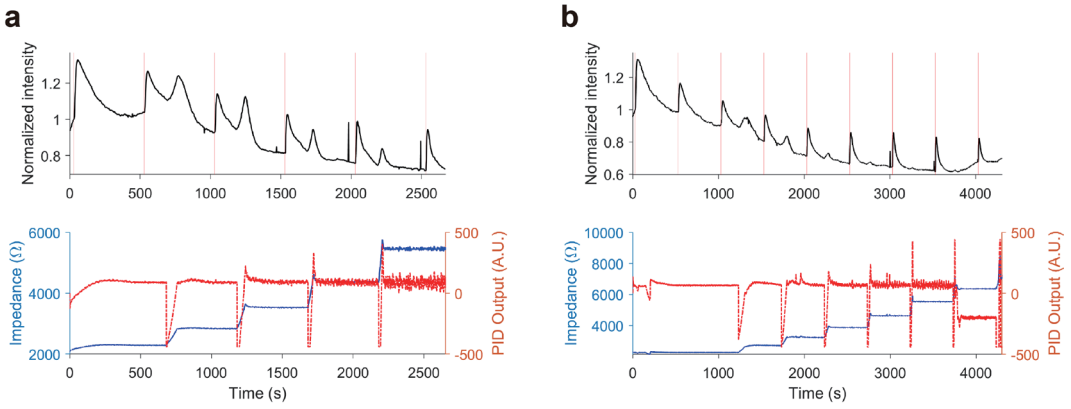

Fig. 5. (Color online) Impedance variation during experiment. (a) Adjustable impedance during experiment. The odor stimulation was 0.4 s 1% 1-octen-3-ol headspace vapor. The red vertical lines indicate the timing of vapor exposure. (b) The PID output became negative when the impedance set point was very high (6569 Ω). In this experiment, the initial impedance set point was 2200 Ω and the impedance was increased 20% every 500 s. The odor stimulation was 0.4 s 1% 1-octen-3-ol headspace vapor. The red vertical lines indicate the timing of vapor exposure.

generated a negative control signal. Although the current impedance could reach the new set point and the biosensor responded to odor stimulation at 4030 s, this response would not last too many times as the liquid exchange had already terminated. A proper impedance set point that can make the liquid layer sufficiently thin and ensure stable liquid exchange is recommended for direct gas-phase odor detection.[26]

4. Conclusions

In this study, we implemented no control, open-loop control, and closed-loop control methods for biosensor liquid film thickness. The no control method was simple when the biosensor lifetime was short. This technique could be applied to rapid target odorant measurement but was not suitable for long-term continuous monitoring. The open-loop control method only required one pump to compensate for the evaporated water, which prolonged the cell lifetime. The optimal infusion rate, however, was difficult to determine. Thus, the biosensor performance was as poor as that under the no control condition in most cases. The closed-loop control method enabled liquid film thickness maintenance and regulation. The liquid exchange using two syringe pumps enabled the removal of the residual ions and odorant molecules, thereby evidently extending the biosensor lifetime. It was suitable for direct gas-phase odor monitoring with the biosensor, even though it required some peripherals such as an impedance measurement circuit, a microcontroller, and syringe pumps.

To further improve the performance of gas-phase odor biosensors, a compact microfluidic structure is preferred. The liquid exchange would be operated under a liquid film thickness of several micrometers. The liquid layer thickness measurement could be changed from the indirect approach using impedance to other direct measurement methods, e.g., an optical method. We believe that with these improvements, an even better gas-phase odor biosensor could be achieved.

References

1 T. Yamada, H. Sugiura, H. Mimura, K. Kamiya, T. Osaki, and S. Takeuchi: Sci. Adv. **7** (2021) 3. https://doi.org/10.1126/sciadv.abd2013
2 S. Shukla, O. Nakano-Baker, D. Godin, D. MacKenzie, and M. Sarikaya: Sci. Data **10** (2023) 295. https://doi.org/10.1038/s41597-023-02195-y
3 Y. Sukekawa, R. Zhou, S. Niki, E. Kuroda, R. Kanzaki, and H. Mitsuno: IEEE. **10** (2024) 1. https://doi.org/10.1109/SENSORS60989.2024.10784913
4 H. Deng, H. Mitsuno, R. Kanzaki, and T. Nakamoto: IEEE Sens. J. **21** (2021) 21184. https://doi.org/10.1109/jsen.2021.3103286
5 H. Mitsuno, T. Sakurai, S. Namiki, H. Mitsuhashi, and R. Kanzaki: Biosens. Bioelectron. **65** (2015) 287. https://doi.org/10.1016/j.bios.2014.10.026
6 T. Datta-Chaudhuri, R. Araneda, P. Abshire, and E. Smela: Sens. Actuators, B **235** (2016) 74. https://doi.org/10.1016/j.snb.2016.05.048
7 H. Deng, Z. Chen, P. Feng, L. Tian, H. Zong, and T. Nakamoto: Electronics **14** (2025) 1852. https://doi.org/10.3390/electronics14091852
8 H. Deng and T. Nakamoto: Biosensors **13** (2023) 1000. https://doi.org/10.3390/bios13121000
9 H. Deng and T. Nakamoto: Anal. Sens. **4** (2024) 6. https://doi.org/10.1002/anse.202400006
10 D. Choi, S. Lee, D. Baek, S. Kim, J. Shin, Y. Choi, Y. Cho, S. Bang, J. Park, S. Lee, T. Park, and S. Hong: ACS Sens. **7** (2022) 3399. https://doi.org/10.1021/acssensors.2c01507

11 O. Kwon, H. Song, S. Park, S. Lee, J. An, J. Park, H. Yang, H. Yoon, J. Bae, T. Park, and J. Jang: Nano Lett. **15** (2015) 6559. https://doi.org/10.1021/acs.nanolett.5b02286
12 J. V. Fahy and B. F. Dickey: N. Engl. J. Med. **363** (2010) 2233. https://doi.org/10.1056/NEJMra0910061
13 Y. Fu, H. Xi, D. Wang, B. He, M. Zheng, Y. Zhou, K. Qin, P. Li, S. Sun, and C. Lu: TrAC, Trends Anal. Chem. **182** (2024) 118065. https://doi.org/10.1016/j.trac.2024.118065
14 K. Sato and S. Takeuchi: Angew. Chem. Int. Ed. **53** (2014) 11798. https://doi.org/10.1002/anie.201404720
15 Y. Hirata, Y. Morimoto, E. Nam, and S. Takeuchi: Lab Chip **19** (2019) 1971. https://doi.org/10.1039/c9lc00131j
16 Y. Sukekawa, H. Mitsuno, R. Kanzaki, and T. Nakamoto: Biosens. Bioelectron. **179** (2021) 113053. https://doi.org/10.1016/j.bios.2021.113053
17 Y. Sukekawa, H. Mitsuno, R. Kanzaki, and T. Nakamoto: IEEE Sens. J. **19** (2019) 7192. https://doi.org/10.1109/JSEN.2019.2916377
18 H. Deng, H. Mitsuno, E. Kuroda, S. Niki, R. Kanzaki, and T. Nakamoto: Sens. Actuators, B **401** (2023) 134995. https://doi.org/10.1016/j.snb.2023.134995
19 T. Chen, T. Wardill, Y. Sun, S. Pulver, S. Renninger, A. Baohan, E. Schreiter, R. Kerr, M. Orger, V. Jayaraman, L. Looger, K. Svoboda, and D. Kim: Nature **499** (2013) 295. https://doi.org/10.1038/nature12354
20 T. Auer, M. Khallaf, A. Silbering, G. Zappia, K. Ellis, R. Álvarez-Ocaña, J. Arguello, B. Hansson, S. Gregory, S. Caron, M. Knaden, and R. Benton: Nature **579** (2020) 402. https://doi.org/10.1038/s41586-020-2073-7
21 H. Deng, H. Mitsuno, R. Kanzaki, S. Nomoto, and T. Nakamoto: IEEE Sens. J. **23** (2023) 24169. https://doi.org/10.1109/jsen.2023.3309968
22 H. Deng, H. Mitsuno, R. Kanzaki, and T. Nakamoto: Meas. Sci. Technol. **35** (2024) 75105. https://doi.org/10.1088/1361-6501/ad3bdc
23 H. Deng, H. Mitsuno, R. Kanzaki, and T. Nakamoto: Biosens. Bioelectron. **199** (2022) 113887. https://doi.org/10.1016/j.bios.2021.113887
24 H. Deng, H. Mitsuno, R. Kanzaki, and T. Nakamoto: IEEE Sens. J. **22** (2022) 16785. https://doi.org/10.1109/JSEN.2022.3192567
25 H. Kida, Y. Fukutani, J. Mainland, C. de March, A. Vihani, Y. Li, Q. Chi, A. Toyama, L. Liu, M. Kameda, M. Yohda, and H. Matsunami: Nat. Commun. **9** (2018) 4556. https://doi.org/10.1038/s41467-018-06806-w
26 Z. Bao, M. Aleixandre, S. Hasegawa, and T. Nakamoto: IEEE Sens. J. **25** (2025) 42482. https://doi.org/10.1109/JSEN.2025.3622147